

Simulation of CO_2 Sorption from the Gas Stream by the Grain of Soda-Lime Sorbent

Vadim Lisitsa(✉), Tatyana Khachkova, Yaroslav Bazaikin, and Vladimir Derevschikov

Institute of Mathematics SB RAS, Koptug Avenue 4, 630090 Novosibirsk, Russia
lisitsavv@ipgg.sbras.ru

Abstract. The paper presents a numerical algorithm for conjugated reactive transport at two spatial scales, in application to $C0_2$ chemosorption. Transport at the macroporous scale (intergranular space) is supported by both the fluid flow and diffusion. At the microporous scale diffusion is assumed as the only transport mechanism. The mathematical model used in this research operates with two parameters that are unavailable from laboratory measurements, they are reaction rate and diffusion coefficient in the microporous space. We present a series of numerical experiments to calibrate these parameters to match the laboratory-measured rates of the concentration changes rates.

Keywords: Chemosorption · Reactive transport · Finite differences · Immersed boundary conditions

1 Introduction

The development of technology for carbon dioxide sorption from gas mixtures by sorbents has been an important engineering task for more than a hundred years, and interest in it is growing every year. Solid CO_2 sorbents based on soda-lime are broadly used in medical applications (inhalation anesthesia, respiratory care), hyperbaric chambers, underwater diving gear, fire safety apparatuses, and mine rescue equipment. The overall reaction of the CO2 sorption process by the soda-lime sorbent can be expressed as follows: $Ca(OH)_2 + CO_2 \rightarrow CaCO_3 \downarrow + H_2O$. Soda-lime sorption performance is mainly affected by the physical and chemical properties of the material, including the shape and the size of particles, porosity, surface area, and hydrodynamic conditions, such as gas velocity, CO_2 concentration, temperature, and humidity [2].

Computational fluid dynamics is a powerful tool for the simulation of chemical reactors. However, for gas-solid reactors such as sorption of CO_2 by solid

The research was done under the support of RSCF grant no. 21-71-20003. Numerical simulations were performed using the supercomputer facilities of Siant-Petersburg Polytechnic University.

© The Author(s), under exclusive license to Springer Nature Switzerland AG 2022
O. Gervasi et al. (Eds.): ICCSA 2022 Workshops, LNCS 13382, pp. 334–347, 2022.
https://doi.org/10.1007/978-3-031-10592-0_25

sorbent grains in fixed beds, geometric complexity has so far prevented detailed modeling of their hydrodynamics. A special approach is needed that is general enough to be applicable for reactor design purposes, but that retains the detailed flow modeling that considers the transport of chemical species and the local concentration gradients in the sorbent grains that could influence reaction kinetics [4].

The current study aims to develop a realistic mathematical model for simulating hydrodynamics and kinetics of CO_2 sorption from the gas stream by the grain of the soda-lime sorbent and to validate the model with the experimental data.

2 Statement of the Problem

We consider two-scale porous media where we distinguish between the large- and small-scale pores. By the large scale pores, we assume those of the size of a few millimeters, whereas the small-scale pores are about several μm. Thus, we suggest that the large-scale pores may support the fluid flow. We assume both advection and diffusion of chemical species take place in the large-scale pores. On the contrary, the small-scale pores do not let the fluid flow through. Thus, the only transport mechanism at this scale is diffusion. This type of problem is also known as conjugate transport. We consider the fluid flow in macro-pores supporting the transport of chemical species. This flow satisfies the steady-state Stokes equation:

$$\begin{array}{ll} \nabla p - \mu \Delta \vec{u} = 0, & \vec{x} \in D_p \\ \nabla \cdot \vec{u} = 0, & \vec{x} \in D_p, \\ \vec{u} = 0, & \vec{x} \in D_g, \end{array} \tag{1}$$

where p is the pressure, u is the fluid flow (averaged over the cell), μ is fluid viscosity, D_p is the macropore space, and D_g is the grain microporous space. Due to the assumption that the microporous space does not support the fluid flow we may avoid solving Stokes-Brikmann equation [6], but Stokes equation has to be solved in the macropore space with the following boundary conditions:

$$\begin{array}{c} Q(x_1^{in}) = \int_{x_2,x_3} v_1(x_1^{in}, x_2, x_3) dx_2 dx_3 = Q_{in}, \\ p(x_1^{out}) = p^{out}, \\ \vec{u} = 0, \vec{x} \in \partial D_p / (x_1 = x_1^{in} \cup x_1 = x_1^{out}), \end{array} \tag{2}$$

where ∂D_p is the boundary of the macropore space.

The reactive transport at both pore scales satisfies the advection-diffusion-reaction equation:

$$\frac{\partial}{\partial t}(\phi C_j) + \nabla \cdot (\vec{u} C_j) - \nabla \cdot (D \nabla C_j) = g_j, \tag{3}$$

where C_j is the molar concentration of the species, ϕ is the micro-porosity, D is the effective diffusion coefficient, and g_j is the external term due to the chemical reaction. Note, that for the macroporous space; i.e., for $\vec{x} \in D_p$ the parameters

are $\phi = 1$, $\vec{u} \neq 0$ is the flow velocity, and $D = D_0$ is the molecular diffusion coefficient of the species. For the microporous material; i.e., for $\vec{x} \in D_g$ we have $\phi < 1$, $\vec{u} \equiv 0$, and $D = \phi D_0/F$, where $F \in [1; 10]$ is the form factor of the micropore space [8]. Below we clarify the particular values of the considered parameters.

We consider two types of species. First is the mobile species which may be transferred by the advection-diffusion reaction 3. Let us denote them as C_m, with $m = 1, ..., M$. The second set is the immobile species which are solids forming the matrix of the sorbent, they are denoted by C_i, with $i = M + 1, ..., J$, where J is the total number of species.

In our considerations we will use the following initial conditions:

$$\begin{array}{l} C_j(\vec{x}, 0) = 0, \quad \vec{x} \in D_p,\ i = 1, ..., J; \\ C_m(\vec{x}, 0) = 0, \quad \vec{x} \in D_g,\ m = 1, ..., M; \\ C_i(\vec{x}, 0) = C_i^0,\ \vec{x} \in D_g,\ i = M + 1, ..., J \end{array}$$

These conditions mean that no species are present in the macroporous space at the beginning, whereas immobile solid species may form the sorbent matrix.

The boundary conditions are made to support the mobile species concentration at the inlet and free outward transport at the outlet.

$$\begin{array}{ll} C_m(x_1^{in}, t) = C_m^{in},\ \vec{x} \in x_1^{in} & m = 1, ..., M; \\ \frac{\partial C_m}{\partial \vec{n}}(\vec{x}, t) = 0, \quad \vec{x} \in x_1^{out} \cup S_{ext} & m = 1, ..., M; \end{array}$$

where S_{ext} is the outer boundaries of the computational domain without inlet and outlet (sides of the reactor). Additionally, we need to specify, that concentrations and fluxes are about to coincide at the interfaces ∂D_p, however, we are using the heterogeneous formulation, so that Eq. (3) is valid everywhere in D but the coefficients are discontinuous.

In this research, we are focused on the particular chemical reaction:

$$Ca(OH)_2 + CO_2 \rightarrow CaCO_3 + H_2O$$

the mobile species are CO_2 and H_2O, whereas $Ca(OH)_2$ and $CaCO_3$ are immobile species. This is the first-order reaction, thus equations for the species become as follows:

$$\begin{array}{c} \frac{\partial}{\partial t}\left(\phi C_{CO_2}\right) + \nabla \cdot \left(\vec{u} C_{CO_2}\right) - \nabla \cdot \left(D_{CO_2} \nabla C_{CO_2}\right) = -k\phi C_{CO_2} C_{Ca(OH)_2}, \\ \frac{\partial}{\partial t}\left(\phi C_{H_2O}\right) + \nabla \cdot \left(\vec{u} C_{H_2O}\right) - \nabla \cdot \left(D_{H_2O} \nabla C_{H_2O}\right) = k\phi C_{CO_2} C_{Ca(OH)_2}, \\ \frac{\partial}{\partial t}\left(C_{Ca(OH)_2}\right) = -k\phi C_{CO_2} C_{Ca(OH)_2}, \\ \frac{\partial}{\partial t}\left(C_{CaCO_3}\right) = k\phi C_{CO_2} C_{Ca(OH)_2}, \end{array} \tag{4}$$

In these notations, k is the reaction rate, and the particular form of the right-hand side is defined by the reaction kinetics. Reaction rate may depend on numerous factors, such as temperature, specific surface of the micropores, etc. We restrict our considerations with the isothermal case with a constant reaction rate. Note, that we consider the concentrations of the gases measured in a free volume, thus they are multiplied by the porosity in Eqs. (4), whereas the concentrations

of the solids are measured for the porous material (not the matrix); thus we do not need to scale them. Also, note that H_2O does not affect the reaction rate or the transport of the species, thus it can be excluded from further considerations.

The initial and boundary conditions can be rewritten as follows:

$$\begin{array}{c} C_{CO_2} = C^{in}_{CO_2}, \quad \vec{x} \in x^{in}_1 \\ \frac{\partial C_{CO_2}}{\partial \vec{n}} = 0, \quad \vec{x} \in x^{out}_1 \cup S_{ext} \end{array} \tag{5}$$

$$\begin{array}{cc} C_{CO_2}(0,\vec{x}) = 0, & \vec{x} \in D_p \cup D_g, \\ C_{Ca(OH)_2}(0,\vec{x}) = 0, & \vec{x} \in D_p, \\ C_{Ca(OH)_2}(0,\vec{x}) = C^0_{Ca(OH)_2}, & \vec{x} \in D_g, \\ C_{CaCO_3}(0,\vec{x}) = 0, & \vec{x} \in D_p, \\ C_{CaCO_3}(0,\vec{x}) = C^0_{CaCO_3}, & \vec{x} \in D_g, \end{array} \tag{6}$$

3 Numerical Methods

3.1 Level-Set

To be able to deal with irregular boundaries of the computational domain (reactor) and the macro-pore space geometry, so that the boundaries of the pore space D_p are not aligned with the grid lines we suggest using the level-set method [5,10,13,15]. Moreover, we are dealing with two level-sets to distinguish between the exterior of the reactor where no flow no diffusion is allowed and the sorbent grains with micropores:

$$\varphi^p(\vec{x}) : \begin{cases} \varphi^p(\vec{x}) > 0, \vec{x} \in D_p, \\ \varphi^p(\vec{x}) < 0, \vec{x} \in D_g \cup D_e, \end{cases} \quad \varphi^e(\vec{x}) : \begin{cases} \varphi^e(\vec{x}) > 0, \vec{x} \in D_p \cup D_g, \\ \varphi^e(\vec{x}) < 0, \vec{x} \in D_e, \end{cases}$$

where D_e is the exterior of the model, which is critical if a cylindrical reactor is considered. The level-sets are needed to be computed only ones at the preliminary step of the algorithm.

3.2 Solving Stokes Equation

To construct spatial approximation of the Stokes Eq. (1), we use the staggered grid scheme. The grid-functions are defined as $p_{i,j,k} = p(ih_1, jh_2, kh_3)$, $(u_1)_{i+1/2,j,k} = u_1((i+1/2)h_1, jh_2, kh_3)$, $(u_2)_{i,j+1/2,k} = u_2(ih_1, (j+1/2)h_2, kh_3)$, $(u_3)_{i,j,k+1/2} = u_3(ih_1, jh_2, (k+1/2)h_3)$ $\varphi^m_{i,j,k} = \varphi^m(ih_1, jh_2, kh_3)$, where h_1, h_2, and h_3 are the spatial steps and $m \in \{p, e\}$. The pore space D_p is defined as $\varphi^p(\vec{x}) > 0$ and the interface ∂D_p corresponds to $\varphi^p(\vec{x}) = 0$.

To approximate Stokes equation we use second order finite-difference scheme:

$$\begin{array}{ll} \mu L[u_1]_{i+1/2,j,k} - D^c_1[p]_{i+1/2,j,k} = 0, & if\ \varphi^p_{i+1/2,j,k} > 0, \\ \mu L[u_2]_{i,j+1/2,k} - D^c_2[p]_{i,j+1/2,} = 0, & if\ \varphi^p_{i,j+1/2,k} > 0, \\ \mu L[u_3]_{i,j,k+1/2} - D^c_3[p]_{i,j,k+1/2} = 0, & if\ \varphi^p_{i,j,k+1/2} > 0, \\ D^c_1[u_1]_{i,j,k} + D^c_2[u_2]_{i,j,k} + D^c_3[u_3]_{i,j,k} = 0, & if\ \varphi^p_{i,j,k} > 0, \end{array} \tag{7}$$

where

$$L[f]_{I,J,K} = D_1^2[f]_{I,J,K} + D_2^2[f]_{I,J,K} + D_2^2[f]_{I,J,K} \tag{8}$$

is the approximation of the Laplace operator with

$$D_1^2[f]_{I,J,K} = \frac{f_{I+1,J,K} - 2f_{I,J,K} + f_{I,J,K}}{h_1^2} = \left.\frac{\partial^2 f}{\partial x_1^2}\right|_{I,J,K} + O(h_1^2), \tag{9}$$

and D_j^c is the approximation of j-th component of the divergence operator

$$D_1^c[f]_{I,J,K} = \frac{f_{I+1/1,J,K} - f_{I,J-1/2,K}}{h_1} = \left.\frac{\partial f}{\partial x_1}\right|_{I,J,K} + O(h_1^2). \tag{10}$$

Here, indices I, J, and K can be either integer or half-integer, but i, j, and k are integers only. The operators approximating derivatives with respect to the other spatial direction can be obtained by the permutations of the role of spatial indices.

Equations (1) are valid only for the internal points of the domain D_p; i.e., if all the points from a stencil belong to pore space. Otherwise we suggest applying the immersed boundary method [7,9,10,12], where the undefined solution at points from D_g and D_e is extrapolated from the neighbouring points in D_p. Details of the immersed boundary conditions implementation is presented in [10].

To resolve the discretized Stokes equation, we compute the steady-state solution of the time-dependent Navier-Stokes equation by the projection method [1]. This approach requires solving the Poisson equation for the pressure, which can be efficiently done using Krylov-type methods with appropriate preconditioner [8], based on the pseudo-spectral approximation [14].

Note that for the simulation of the chemical species transport we need to state the flow rate equal to zero inside the grains and in the exterior part of the domain which means that

$$\begin{aligned}
(u_1)_{i+1/2,j,k} &= 0,\ if\ \varphi^p_{i+1/2,j,k} \le 0,\\
(u_2)_{i,j+1/2,k} &= 0,\ if\ \varphi^p_{i,j+1/2,k} \le 0,\\
(u_3)_{i,j,k+1/2} &= 0,\ if\ \varphi^p_{i,j,k+1/2} \le 0.
\end{aligned}$$

3.3 Solution of the Advection-Diffusion-Reaction Equation

To solve advection-diffusion-reaction equations we use the splitting scheme, in particular, we solve the advection-diffusion equation using an explicit in time scheme and then solve the reactive part of the equation applying a semi-implicit scheme.

Let us state $C^n_{i,j,k} = C(ih_1, jh_2, kh_3, n\tau)$, where τ is the temporal step. After that the advection-diffusion equation is approximated by the explicit in time scheme. We use the first-order approximation in time, second-order approximation of the diffusive part and the third-order WENO scheme to approximate advective part [11,15,16]:

$$\frac{\tilde{C}^{n+1}_{i,j,k}-C^n_{i,j,k}}{\tau}+D^3_1[u_1C]^n_{i,j,k}+D^3_2[u_2C]^n_{i,j,k}+D^3_3[u_3C]^n_{i,j,k}-[\nabla_h\cdot(D\nabla_hC)]^n_{i,j,k}=0,\quad \varphi^e_{i,j,k}>0, \tag{11}$$

where

$$D^3_1[u_1C]^n_{i,j,k}=\frac{F_1[C,\vec{u}]_{i+1/2,j,k}-F_1[C,\vec{u}]_{i_1-1/2,j,k}}{h}. \tag{12}$$

The fluxes are defined as

$$F_1[C,\vec{u}]_{j_1\pm1/2,j_2j_3}=\begin{cases}F_1^-[C]_{j_1\pm1/2,j_2,j_3},\ if\ (u_1)_{j_1\pm1/2,j_2,j_3}<0,\\ F_1^+[C]_{j_1\pm1/2,j_2,j_3},\ if\ (u_1)_{j_1\pm1/2,j_2,j_3}>0,\end{cases}$$

where

$$F_1^{\pm}[C]_{j_1+1/2,j_2,j_3}=(u_1)_{j_1+1/2,j_2,j_3}\left[(w_1)^{\pm}_1(p_1)^{\pm}_1+(w_1)^{\pm}_2(p_1)^{\pm}_2\right],$$

$$(p_1)^{\pm}_1=-\frac{(\delta_1)^{\pm}_{j_1-1,j_2,j_3}}{2}+\frac{3(\delta_1)^{\pm}_{j_1,j_2,j_3}}{2},\ (p_1)^{\pm}_2=\frac{(\delta_1)^{\pm}_{j_1,j_2,j_3}}{2}+\frac{(\delta_1)^{\pm}_{j_1+1,j_2,j_3}}{2},$$

$$(\delta_1)^-_{j_1-1,j_2,j_3}=C_{j_1+2,j_2,j_3},\ (\delta_1)^-_{j_1,j_2,j_3}=C_{j_1+1,j_2,j_3},\ \ (\delta_1)^-_{j_1+1,j_2,j_3}=C_{j_1,j_2,j_3},$$
$$(\delta_1)^+_{j_1-1,j_2,j_3}=C_{j_1-1,j_2,j_3},\ \ (\delta_1)^+_{j_1,j_2,j_3}=C_{j_1,j_2,j_3},\ \ (\delta_1)^+_{j_1+1,j_2,j_3}=C_{j_1+1,j_2,j_3}.$$

The weights for the third-order WENO scheme are defined as

$$(w_1)^{\pm}_l=\frac{\gamma_l}{(\varepsilon^{\pm}_1+(S_1)^{\pm}_l)^2}\frac{1}{\sum_{k=1}^2\gamma_k(\varepsilon^{\pm}_1+(S_1)^{\pm}_k)^{-2}},$$

where $l=1,2$. The smoothers are

$$(S_1)^{\pm}_1=\left((\delta_1)^{\pm}_{j_1,j_2,j_3}-(\delta_1)^{\pm}_{j_1-1,j_2,j_3}\right)^2,\ (S_1)^{\pm}_2=\left((\delta_1)^{\pm}_{j_1+1,j_2,j_3}-(\delta_1)^{\pm}_{j_1,j_2,j_3}\right)^2,$$

$$\gamma_1=\tfrac{1}{3},\ \gamma_2=\tfrac{2}{3},$$

and

$$\varepsilon^{\pm}_1=10^{-6}\max\left\{((\delta_1)^{\pm}_{j_1-1,j_2,j_3})^2,((\delta_1)^{\pm}_{j_1,j_2,j_3})^2,((\delta_1)^{\pm}_{j_1+1,j_2,j_3})^2\right\}+10^{-99}.$$

Operators, approximating the derivatives to the other spatial direction, can be obtained using the spatial indices' permutation.

For the operator $[\nabla_h\cdot(D\nabla_hC)]^n_{i,j,k}$ we consider one term; i.e., $\frac{\partial}{\partial x_1}\left(D\frac{\partial}{\partial x_1}\right)$, the other two can be constructed in the similar manner.

$$\frac{\partial}{\partial x_1}\left(D\frac{\partial}{\partial x_1}\right)\approx\frac{1}{h_1}\left[\tilde{D}_{i+1/2,j,k}\frac{C^n_{i+1,j,k}-C^n_{i,j,k}}{h_1}-\tilde{D}_{i-1/2,j,k}\frac{C^n_{i,j,k}-C^n_{i-1,j,k}}{h_1}\right],$$

where

$$D_{i+1/2,j,k}=2\left(D^{-1}_{i+1,j,k}+D^{-1}_{i,j,k}\right)^{-1}.$$

This operator is constructed based on the theory of conservative schemes [17]. It is second-order accurate if the coefficients are constant, however, in some cases of discontinuous coefficients it may degenerate to the first order.

The next step of the splitting scheme is the solution correction due to the reactive term. Consider the system of ordinary differential equations:

$$\begin{gathered}\frac{\partial}{\partial t}\left(\phi C_{CO_2}\right) = -k\phi C_{CO_2} C_{Ca(OH)_2},\\ \frac{\partial}{\partial t}\left(C_{Ca(OH)_2}\right) = -k\phi C_{CO_2} C_{Ca(OH)_2},\\ \frac{\partial}{\partial t}\left(\phi C_{H_2O}\right) = k\phi C_{CO_2} C_{Ca(OH)_2},\\ \frac{\partial}{\partial t}\left(C_{CaCO_3}\right) = k\phi C_{CO_2} C_{Ca(OH)_2}.\end{gathered} \tag{13}$$

The system should be integrated at the time interval $t \in [t^n, t^{n+1}]$. We suggest using a simple semi-implicit scheme to resolve the system (13), which allows using arbitrary large time steps.

$$\begin{gathered}\frac{C^{n+1}_{CO_2} - \tilde{C}^{n+1}_{CO_2}}{dt} = -kC^{n+1}_{CO_2}\tilde{C}^{n+1}_{Ca(OH)_2},\\ \frac{C^{n+1}_{Ca(OH)_2} - \tilde{C}^{n+1}_{Ca(OH)_2}}{dt} = -k\varphi\tilde{C}^{n+1}_{CO_2}C^{n+1}_{Ca(OH)_2},\\ \frac{C^{n+1}_{H_2O} - \tilde{C}^{n+1}_{H_2O}}{dt} = kC^{n+1}_{CO_2}C^{n+1}_{Ca(OH)_2},\\ \frac{C^{n+1}_{CaCO_3} - \tilde{C}^{n+1}_{CaCO_3}}{dt} = k\varphi C^{n+1}_{CO_2}C^{n+1}_{Ca(OH)_2},\end{gathered}$$

The obtained scheme is the first order accurate and unconditionally stable. However, the time steps $dt \leq \tau$ are chosen to preserve the prescribed accuracy level.

4 Experiments

In this research, we present a series of numerical experiments to calibrate the mathematical model to match the sorbent properties measured in a lab. Soda-lime Loflosorb (Intersurgical Ltd, UK) is a commercially available CO_2 sorbent that is used in breathing systems to absorb exhaled carbon dioxide during anesthesia. Loflosorb contains an indicator that turns from white to purple upon exhaustion of the sorbent. Loflosorb contains 60 wt% of $Ca(OH)_2$, 15 wt% of water, and less than 0.1 wt% of the indicator (ethyl violet). Loflosorb sorbent pellets are spherical particles 3 mm in diameter [3]. The mass density of the granules, porosity (measured in m^3/kg), and mass fraction of H_2O, $Ca(OH)_2$ and $CaCO_3$ at the initial stage were measured in a lab. They are provided in Table 1.

Table 1. Measured properties of the sorbent at the initial stage.

Property	Notation	Loflosorb
Density (kg/m^3)	ρ	1080
Chem. porosity (m^3/kg)	v_p	$4.6 \cdot 10^{-4}$
Mass fraction of $Ca(OH)_2$	$\mu_{Ca(OH)_2}$	0.76
Mass fraction of $CaCO_3$	μ_{CaCO_3}	0.05

4.1 Lab Experiments

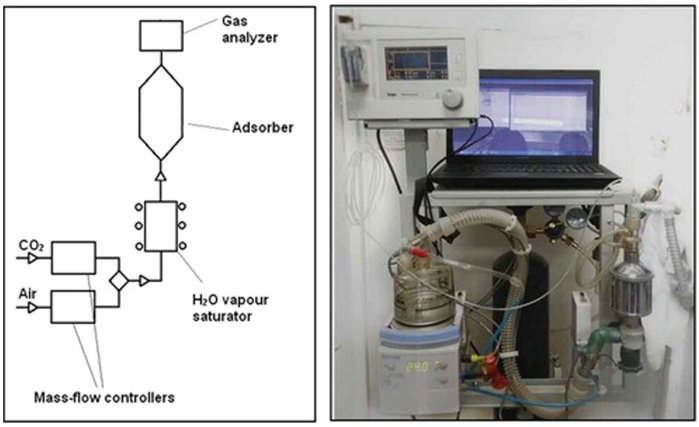

Fig. 1. Experimental setup for CO_2 chemisorption measurement: scheme - left, photo - right.

Carbon dioxide chemisorption from the gas mixtures was studied in the experimental setup shown in Fig. 1. The process of CO_2 chemisorption by samples of the soda-lime sorbent (Loflosorb, Intersurgical Ltd. and ($m_s = 3$ g) was carried out in the differential reactor mode. The granules of the sample were distributed evenly in one layer along the grid of the reactor. The gas-air mixture with a constant CO_2 content (1 vol. % or 5 vol. %) was passed through the reactor with the inlet flow rate of 100 L/h at 37°C. Each sample was kept in contact with the gas-air mixture for a specified time, after that, it was removed from the reactor and placed into the sealed container.

Elemental analysis of the sorbent samples before and after chemisorption was performed using the ARL Perform'X (Thermo Scientific) X-Ray Fluorescence Spectrometer. The chemical composition of the sorbent samples was studied by synchronous thermal analysis method (thermogravimetry (TG) coupled with differential thermal analysis (DTA)) using the STA 449 Jupiter instrument (Netzsch, Germany). The weight contents of $Ca(OH)_2$ and $CaCO_3$ were calculated from the mass loss effects around 450 and 750°, respectively. Results of laboratory measurements are provided in Table 2.

4.2 Relations Between Laboratory and Simulated Data

However, the mathematical model operates with dimensionless porosity and molar concentrations. To estimate the dimensionless porosity ϕ we need to consider the measured one v_p and the mass density of the microporous material ρ.

Table 2. Measured mass fractions of $Ca(OH)_2$ and $CaCO_3$ at different time instants

CO_2 concentration 5%				
	$t = 0$	$t = 15$	$t = 30$	$t = 60$
$\mu_{Ca(OH)_2}$	0.76	0.32	0.19	0.13
μ_{CaCO_3}	0.05	0.5	0.72	0.78
CO_2 concentration 1%				
	$t = 0$	$t = 15$	$t = 30$	$t = 60$
$\mu_{Ca(OH)_2}$	0.6948	0.4604	0.3535	0.2672
μ_{CaCO_3}	0.0522	0.2318	0.3818	0.475

If a fixed volume V of the material is given, its mass is $m_g = V\rho$, and the pore volume is $V_p = m_g v_p = V\rho v_p$. Thus, the dimensionless porosity can be found as:

$$\phi = \frac{V_p}{V} = \rho v_p.$$

The solid materials in the porous composite are defined by their mass ratio:

$$\mu_j = \frac{m_j}{m_c} = \frac{\rho_j V}{\rho V} = \frac{\rho_j}{\rho},$$

where ρ_j is the mass concentration in a unit volume of porous material (not matrix!) and ρ is the mass density of porous material. In these notations j can be either $Ca(OH)_2$ or $CaCO_3$. After that, the molar concentration can be computed as

$$C_j = \frac{\rho_j}{M_j} = \frac{\mu_j \rho}{M_j},$$

where M_j is the molar mass of the species.

The chemical reaction changes concentrations of the species which causes changes in the physical properties of the microporous material, including porosity and mass density which are important for the mass fraction estimation.

Porosity Change. Assume the initial porosity is φ^0, initial mass density of the porous material is ρ^0, mass fractions of $Ca(OH)_2$ and $CaCO_3$ are $\mu^0_{Ca(OH_2)}$, and $\mu^0_{CaCO_3}$ respectively. Thus, molar concentrations can be computed and assumed to be known at the initial stage as $C^0_{Ca(OH)_2}$ and $C^0_{CaCO_3}$. Consider a volume of the porous material V, then the masses of $Ca(OH)_2$ and $CaCO_3$ in this volume are

$$m^0_j = C^0_j M_j V,$$

where can be either $Ca(OH)_2$ or $CaCO_3$. The initial volumes of the species are

$$V^0_j = \frac{C^0_j M_j V}{r_j},$$

where r_j is the mass density of pure species, as provided in Table 3.

Table 3. Physical parameters of pure species

Property	Notation	CO_2	H_2O	$Ca(OH)_2$	$CaCO_3$
Molar mass (kg/mol)	M	0.044	0.018	0.074	0.1
Crystals density (kg/m^3)	r_j	–	1000	2240	2710
Diffusion coefficient (m^2/s)	D	$1.5 \cdot 10^{-5}$	–	–	–

Thus, we may define the unchangeable substance volume as

$$V_c = V(1-\varphi^0) - \sum_j V_j = V(1-\varphi^0) - \sum_j \frac{C_j^0 M_j V}{r_j}.$$

If the reaction takes place, the concentrations changes, thus, the volumes of the species change accordingly and the matrix volume is

$$\begin{gathered} V_m = V_c + \textstyle\sum_j V_j \\ = V(1-\varphi^0) - \textstyle\sum_j \frac{C_j^0 M_j V}{r_j} + \sum_j \frac{C_j M_j V}{r_j} \\ = V(1-\varphi^0) - \textstyle\sum_j \frac{(C_j - C_j^0) M_j V}{r_j}. \end{gathered}$$

Thus the porosity as a function of concentrations can be represented as

$$\varphi(C_{Ca(OH)_2}, C_{CaCO_3}) = 1 - \frac{V_m}{V} = \varphi^0 - \sum_j \frac{(C_j - C_j^0) M_j}{r_j}.$$

This equation should also be closed by the extra equation according to the reaction:

$$C_{Ca(OH)_2} + C_{CaCO_3} = const = C^0_{Ca(OH)_2} + C^0_{CaCO_3},$$

which allows considering porosity as a function of one independent variable.

Density Change. To estimate the changes in the density of the granules, consider a volume V. Same as above, assume the density of the porous material ρ^0, the concentrations $C^0_{Ca(OH)_2}$ and $C^0_{CaCO_3}$, and mass fractions $\mu^0_{Ca(OH)_2}$ and $\mu^0_{CaCO_3}$ are known at the initial stage. Thus, the mass of the unchanged component is

$$m_c = (1 - \sum_j \mu_j^0)\rho^0 V = (\rho^0 - \sum_j C_j^0 M_j)V$$

This mass does not change during the reaction, whereas masses of $Ca(OH)_2$ and $CaCO_3$ do. Thus, the mass of the material changes as

$$\begin{gathered} m_m = m_c + \textstyle\sum_j m_j \\ = (\rho^0 - \textstyle\sum_j C_j^0 M_j)V + \sum_j C_j M_j V = \rho^0 V + \sum_j (C_j - C_j^0) M_j V \end{gathered}$$

and the mass density is

$$\rho(C_{Ca(OH)_2}, C_{CaCO_3}) = \rho^0(C^0_{Ca(OH)_2}, C^0_{CaCO_3}) + \textstyle\sum_j (C_j - C_j^0) M_j$$

Mass Fraction. Having estimated the molar concentrations of the species one can estimate the mass fraction as

$$\mu_j(C_{Ca(OH)_2}, C_{CaCO_3}) = \frac{C_j M_j}{\rho(C_{Ca(OH)_2}, C_{CaCO_3})}.$$

4.3 Results of Simulation

In our simulations, we considered a reduced reactor model of the diameter 15 mm and length also equal to 15 mm. The granule of the diameter of 3 mm is placed in the middle of the reactor. The flow rate was $1.73 \cdot 10^{-6}\,\mathrm{m}^3/\mathrm{s}$, which ensures the same fluid flow velocity in the middle of the reactor as in the lab experiment. Note, that reduction of the reactor size does not affect the results of the experiment, because the granule is far from the reactor sides, thus the flow is not affected by the side effects. The grid step is 0.3 mm; which is 10 grid points per granule. The size of the model is 50^3 points. To simulate the conjugated reactive transport we need to define the fluid viscosity (Eq. (1)), which is $\mu = 2.8 \cdot 10^{-4}$ the dynamic viscosity of air at normal conditions; the diffusion coefficient for CO_2 in the air is $D_0 = 1.5 \cdot 10^{-5}\,\mathrm{m}^2/\mathrm{s}$. The diffusion coefficient in the microporous media, used in Eq. (3), is defined as $D = \phi D_0/F$, where ϕ is the dimensionless porosity, which is 0.49 at the initial stage for considered material. However, the parameter F is the formation factor, which characterizes the complexity of the pore space [8]. Originally it was defined as the ratio of the electric resistivity of the fluid to that of the porous material filled with this fluid. However, the same relations are valid for diffusion coefficient and thermal conductivity. Formation factor is not available from the lab measurements, but usually, it varies between 1 and 10, and it is approximately 2–4 for such high porosity. In this research, we study the effect of the formation factor on the CO_2 sorption and calibrate this parameter to match the experimental data. The other unknown parameter is the reaction rate k measured in $m^3/(mol \cdot s)$. Thus, our numerical experiments are done to calibrate two model parameters: the formation factor and the reaction rate. In particular we considered $F = 1, 2, ..., 10$ and $k \in \{10^{-4}, 10^{-3}, 10^{-2}, 10^{-1}\}$.

Following the lab experiment, we considered two cases of CO_2 concentration at the inlet. It is typically defined via volumetric fraction ξ_{CO_2}. At normal conditions, one mole of gas fills in 22.4 liters, thus molar concentration can be derived as

$$C_{CO_2} = \frac{\xi_{CO_2}}{22.4} 10^3 \quad mol/m^3.$$

We deal with volumetric concentrations of 5% and 1% which correspond to $2.2321\,\mathrm{mol}/\mathrm{m}^2$ and $0.4464\,\mathrm{mol}/\mathrm{m}^3$, respectively. Presented experiments illustrate that values of $k = 10^{-4}$ and $k = 10^{-3}$ are too small to match experimental data. In particular, if $k = 10^{-4}$ concentrations changes almost linearly in time up to 7200 s (2 h) (Figs. 2, 3, 4 and 5).

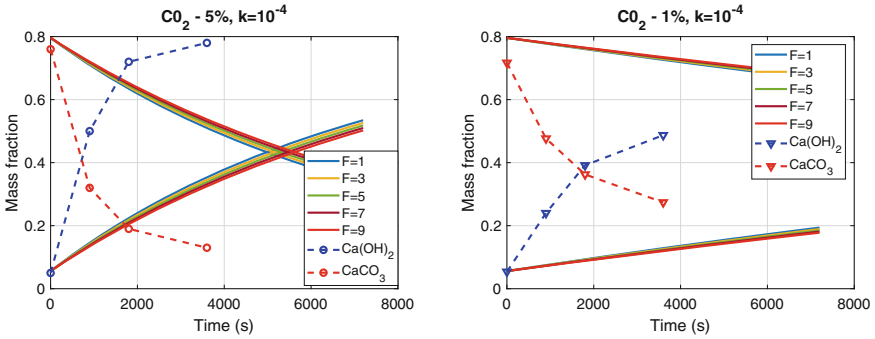

Fig. 2. Mass fraction of $Ca(OH)_2$ and $CaCO_3$ in the granule for different values of formation factor and fixed reaction rate $k = 10^{-4}$. Left plot corresponds to CO_2 volume concentration equal to 5%, right plot corresponds to 1% of CO_2.

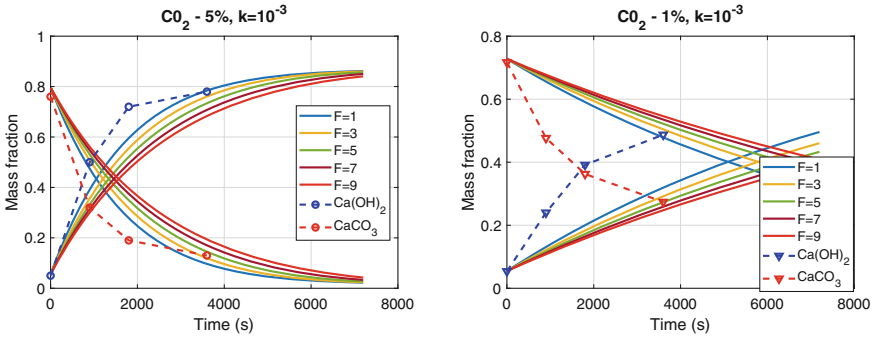

Fig. 3. Mass fraction of $Ca(OH)_2$ and $CaCO_3$ in the granule for different values of formation factor and fixed reaction rate $k = 10^{-3}$. Left plot corresponds to CO_2 volume concentration equal to 5%, right plot corresponds to 1% of CO_2.

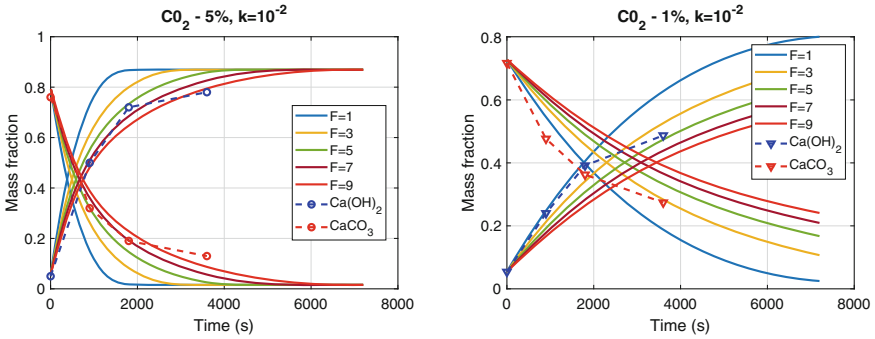

Fig. 4. Mass fraction of $Ca(OH)_2$ and $CaCO_3$ in the granule for different values of formation factor and fixed reaction rate $k = 10^{-2}$. Left plot corresponds to CO_2 volume concentration equal to 5%, right plot corresponds to 1% of CO_2.

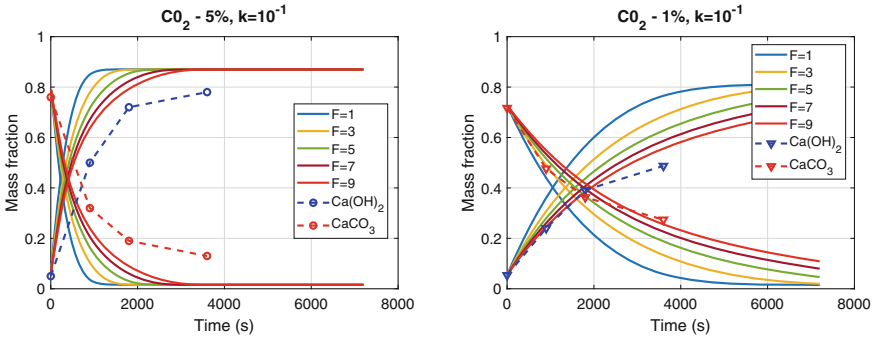

Fig. 5. Mass fraction of $Ca(OH)_2$ and $CaCO_3$ in the granule for different values of formation factor and fixed reaction rate $k = 10^{-1}$. Left plot corresponds to CO_2 volume concentration equal to 5%, right plot corresponds to 1% of CO_2.

5 Conclusions

We presented the numerical algorithm for the reactive transport simulation. The model operates with the conjugated transport at two spatial scales. The macroscale is defined by the size of the sorbent granules, where the fluid flow in the pore space is simulated using Stokes equations. The microscale follows the size of the pores inside the sorbent granules, where we assume no flow, but only the diffusion. However, the diffusion rate in the microporous space is unknown. We assumed CO_2 sorption satisfies the first-order reaction, with unknown reaction rates. In this research, we focused on model calibration, i.e., we performed a series of numerical simulations with different parameters to match the laboratory measurements of the changes in the species concentrations. We figured out that the best matching parameters are the reaction rate equals to $10^2\,\mathrm{m}^2/(\mathrm{mol}\cdot\mathrm{s})$ with the formation factor of the microporous space less than 10.

References

1. Brown, D.L., Cortez, R., Minion, M.L.: Accurate projection methods for the incompressible Navier-Stokes equations. J. Comput. Phys. **168**(2), 464–499 (2001)
2. Derevschikov, V.S., Kazakova, E.D., Yatsenko, D.A., Veselovskaya, J.V.: Multiscale study of carbon dioxide chemisorption in the plug flow adsorber of the anesthesia machine. Sep. Sci. Technol. **56**(3), 485–497 (2021)
3. Derevshchikov, V.S., Kazakova, E.D.: Comparative analysis of the chemical composition and sorption, textural, and strength properties of commercial medical CO_2 sorbents. Catal. Ind. **12**(1), 1–6 (2020). https://doi.org/10.1134/S2070050420010043
4. Dixon, A.G., Nijemeisland, M.: CFD as a design tool for fixed-bed reactors. Ind. Eng. Chem. Res. **40**(23), 5246–5254 (2001)
5. Gibou, F., Fedkiw, R., Osher, S.: A review of level-set methods and some recent applications. J. Comput. Phys. **353**, 82–109 (2018)

6. Hwang, W.R., Advani, S.G.: Numerical simulations of stokes-brinkman equations for permeability prediction of dual scale fibrous porous media. Phys. Fluids **22**(11), 113101 (2010)
7. Johansen, H., Colella, P.: A cartesian grid embedded boundary method for Poisson's equation on irregular domains. J. Comput. Phys. **147**(1), 60–85 (1998)
8. Khachkova, T., Lisitsa, V., Reshetova, G., Tcheverda, V.: GPU-based algorithm for evaluating the electrical resistivity of digital rocks. Comput. Math. Appl. **82**, 200–211 (2021)
9. Li, X., Huang, H., Meakin, P.: Level set simulation of coupled advection-diffusion and pore structure evolution due to mineral precipitation in porous media. Water Resour. Res. **44**(12), W12407 (2008)
10. Lisitsa, V., Bazaikin, Y., Khachkova, T.: Computational topology-based characterization of pore space changes due to chemical dissolution of rocks. Appl. Math. Model. **88**, 21–37 (2020). https://doi.org/10.1016/j.apm.2020.06.037
11. Liu, X.D., Osher, S., Chan, T.: Weighted essentially non-oscillatory schemes. J. Comput. Phys. **115**(1), 200–212 (1994)
12. Luo, K., Zhuang, Z., Fan, J., Haugen, N.E.L.: A ghost-cell immersed boundary method for simulations of heat transfer in compressible flows under different boundary conditions. Int. J. Heat Mass Transf. **92**, 708–717 (2016)
13. Osher, S., Fedkiw, R.P.: Level set methods: an overview and some recent results. J. Comput. Phys. **169**(2), 463–502 (2001)
14. Pleshkevich, A., Vishnevskiy, D., Lisitsa, V.: Sixth-order accurate pseudo-spectral method for solving one-way wave equation. Appl. Math. Comput. **359**, 34–51 (2019)
15. Prokhorov, D., Lisitsa, V., Khachkova, T., Bazaikin, Y., Yang, Y.: Topology-based characterization of chemically-induced pore space changes using reduction of 3D digital images. J. Comput. Sci. **58**, 101550 (2022)
16. Qiu, J.M., Shu, C.W.: Conservative high order Semi-Lagrangian finite difference WENO methods for advection in incompressible flow. J. Comput. Phys. **230**(4), 863–889 (2011)
17. Samarskii, A.A.: The Theory of Difference Schemes. Pure and Applied Mathematics, vol. 240. CRC Press (2001)